Experimental Validation of an Ellipsoidal State Estimation Procedure for a Magnetic Levitation System

Andreas Rauh * **Jonas Soueidan** ** **Simon Rohou** **
Luc Jaulin **

* *Carl von Ossietzky Universität Oldenburg, Department of Computing Science, Group: Distributed Control in Interconnected Systems, D-26111 Oldenburg, Germany (e-mail: Andreas.Rauh@uni-oldenburg.de)*
** *ENSTA Bretagne, Lab-STICC, Robex, 29806 Brest, France (e-mail: jonas.soueidan@ensta-bretagne.org, simon.rohou@ensta-bretagne.fr, lucjaulin@gmail.com)*

Abstract: Set-based state estimation procedures have the advantage of enclosing all possible system states under the assumption of bounded measurement uncertainty, the structural correctness of dynamic systems models, and the representation of external disturbances and imperfectly known parameters by finitely large sets. In contrast to stochastic counterparts, often employing one of the available variants of Kalman filters, set-based approaches are less widely used. The reason for this observation is the fact that naive implementations often suffer from a non-negligible degree of overestimation and that (unless certain monotonicity properties are satisfied) set-based computations come with a notable increase of the computational complexity, resulting among others from required interval splitting procedures. This paper tries to resolve both issues by means of an ellipsoidal implementation of a discrete-time set-valued state estimation procedure that is validated experimentally and compared with an Unscented Kalman Filter (UKF) for a laboratory-scale magnetic levitation system.

Keywords: Set-based state estimation, ellipsoidal state enclosures, bounded uncertainty, nonlinear system models, magnetic levitation systems

1. INTRODUCTION

Set-based state estimation procedures can be classified in general into approaches that rely on a predictor–corrector structure and on formulations that mimic the structure of Luenberger-like observers (Puig et al., 2005).

The first class of estimators is characterized by the use of set-valued calculus, propagating uncertain state domains from one time instant up to that instant at which new measured data become available (Kletting et al., 2006). At this point, set-based intersections are performed with domains that represent the measured states with bounded uncertainty. In general, different set representations have been investigated in the literature, for example, axis-aligned intervals, preconditioned interval boxes, (constrained) zonotopes, ellipsoids, or polygons (Kurzhanskii and Vályi, 1997; Rauh et al., 2021; Rego et al., 2022; Rohou and Jaulin, 2021). Although the use of intervals is simple to implement on the basis of existing software libraries (Krämer, n.a.; Rump, 1999), they suffer from the drawback of overestimation, mostly due to the so-called wrapping effect that arises when complex-shaped domains in the state space are enclosed by axis-aligned boxed that are then further propagated over time (Lohner, 2001). All of the other above-mentioned alternative set representations allow for a reduction of overestimation and for capturing correlations between individual state variables. Especially the ellipsoid approach proposed by Rauh and Jaulin (2021) has the advantage of an effort close to the Extended Kalman Filter. This effort is commonly much smaller than the one of other set-based options. Therefore, the ellipsoidal technique offers the advantages of combining small overestimation and real-time implementability.

The second class of set-based estimators exploits the structure of continuous- and discrete-time Luenberger observers and allows for implementing decoupled state observers for lower and upper bounds of each component of the state vector (Efimov et al., 2013). This requires that the system model under investigation satisfies specific monotonicity properties (Smith, 1995). These properties are satisfied naturally for many thermo-fluidic systems as well as for compartmental models in chemistry, biology, or biomedicine. If this is not the case, as usual for electrical and mechanical systems, time-invariant or time-varying transformations of the state equations are possible to implement interval observers. These transformations typically lead to a certain degree of pessimism that should be avoided to prevent excessively conservative state enclosures (Rauh and Kersten, 2021). Alternatively, the approach suggested in Wang et al. (2018) can be used, which introduces an additional gain matrix in comparison with other interval observers to make it applicable to (quasi-)linear systems not having the required monotonicity property.

This paper is structured as follows. Sec. 2 summarizes the modeling and parameter identification for a laboratory-scale magnetic levitation system. Sec. 3 gives an overview of a UKF and an ellipsoidal state enclosure approach which are both used in Sec. 4 for an experimental state estimation. Finally, conclusions and an outlook on future work are given in Sec. 5.

2. MODELING AND PARAMETER IDENTIFICATION FOR A MAGNETIC LEVITATION SYSTEM

2.1 System Overview

The experimental validation of an ellipsoidal state estimation algorithm and its comparison with a UKF are performed in this paper for a laboratory-scale magnetic levitation system manufactured by INTECO, cf. Fig. 1.

The test bench consists of an electromagnet mounted on the top of the setup that can be actuated with its supply voltage u. The goal is to position a ferromagnetic sphere of mass m in a stable manner at the distance x_1 below the magnet. For a dynamic modeling, the state vector

$$\mathbf{x} = \begin{bmatrix} x_1 & x_2 & x_3 \end{bmatrix}^T \in \mathbb{R}^{n_\mathrm{x}} \tag{1}$$

is introduced, which further contains the sphere's velocity x_2 (positive values correspond to a motion in downward direction) and the electric current x_3 in the magnet.

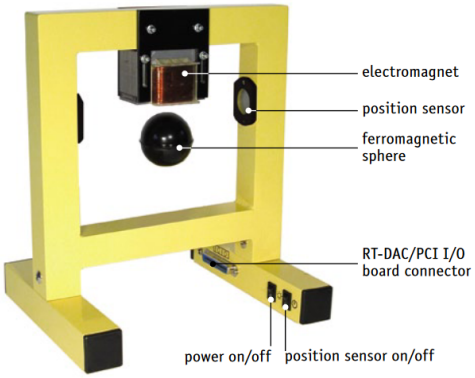

Fig. 1. Magnetic levitation system manufactured by INTECO Sp. z o. o. (n.a.).

As described in numerous other publications dealing with modeling, control, and state estimation for this system, cf. Balko and Rosinova (2017); Rosinova and Hypiusova (2021), a nonlinear set of state equations is given in the form

$$\begin{aligned} \dot{x}_1 &= x_2 \\ \dot{x}_2 &= -\frac{F_\mathrm{em}(x_1, x_3)}{2m} + g \\ \dot{x}_3 &= \frac{1}{f_\mathrm{ip}(x_1)}(k_\mathrm{i} \cdot u + c_\mathrm{i} - x_3) \ , \end{aligned} \tag{2}$$

where

$$F_\mathrm{em}(x_1, x_3) = \frac{F_\mathrm{emP1}}{F_\mathrm{emP2}} \cdot x_3^2 \cdot e^{-\frac{x_1}{F_\mathrm{emP2}}} \tag{3}$$

is an approximation [1] of the actuating force provided by the electromagnet.

[1] As described in Balko and Rosinova (2017), different approximations of the electromagnet's force characteristic can be determined, namely also rational position dependencies. We restrict ourselves to the semi-empirical exponential function because of its simple form and differentiability for all real-valued parameters and state variables which is a prerequisite for the application of the suggested ellipsoidal state estimator. This differentiability requirement is more difficult to satisfy for rational expressions if (although nonphysical) states $x_1 < 0$ may be contained in the conservative enclosures provided by a set-based estimator.

The force of the electromagnet is controlled indirectly by the supply voltage u, leading to a first-order lag behavior of the corresponding current. The time constant of this first-order lag element is position-dependent according to

$$f_\mathrm{ip}(x_1) = \frac{f_\mathrm{ip1}}{f_\mathrm{ip2}} \cdot e^{-\frac{x_1}{f_\mathrm{ip2}}} \ . \tag{4}$$

2.2 Parameter Identification

The parameters F_emP1, F_emP2, f_ip1, f_ip2, k_i, and c_i in (2)–(4) need to be identified experimentally for the desired state estimation purposes. Because both (3) and (4) are semi-empirical approximations of the true (inductance dependent) force and time constant, we aim at enclosing the corresponding parameters by intervals that can be dealt with directly by the ellipsoidal state estimator. Note that these intervals are a means to enhance the model fidelity by accounting for the uncertainty of the parameter identification stage. Due to the fact that the system's open-loop behavior is unstable, the parameter identification consists of two subtasks:

(1) identification of the parameters F_emP1 and F_emP2 in Eq. (3) for stationary closed-loop controlled operating points of the sphere position by using the equilibrium condition

$$F_\mathrm{em} = 2mg \ ; \tag{5}$$

(2) identification of the parameters f_ip1 and f_ip2 in Eq. (4) as well as the values k_i and c_i of the electric subsystem in a controlled system operation with different constant and time-varying position values x_1.

Identification of the Parameters of the Force Characteristic: During the first identification stage, we take into account explicitly the uncertainty of the optical position sensor which consists of random errors of $\pm 0.02\,\mathrm{mm}$ amplitude and an additional offset of $\pm 0.1\,\mathrm{mm}$ resulting from variations of ambient light conditions. The parameters F_emP1 and F_emP2 are obtained by a pairwise comparison of two experiments with different desired constant positions, where the point-valued position sensor readings (after inflation with the interval $[-0.12\,;\,+0.12]$ mm) as well as the current measurement are averaged over a time span of 100 s with a sampling period of 3 ms. Denote the resulting values by $\left[\tilde{x}_1^{\langle \mathrm{A} \rangle}\right]$ and $\left[\tilde{x}_1^{\langle \mathrm{B} \rangle}\right]$ for the position values and by $\tilde{x}_3^{\langle \mathrm{A} \rangle}$ and $\tilde{x}_3^{\langle \mathrm{B} \rangle}$ for the current, respectively.

Then, a division of two evaluations of Eq. (3) according to

$$F_\mathrm{em} = 2mg \in \frac{F_\mathrm{emP1}}{F_\mathrm{emP2}} \cdot \left(\tilde{x}_3^{\langle \iota \rangle}\right)^2 \cdot e^{-\frac{\left[\tilde{x}_1^{\langle \iota \rangle}\right]}{F_\mathrm{emP2}}} \ , \quad \iota \in \{\mathrm{A}, \mathrm{B}\} \tag{6}$$

under the static force condition (5) and resolving it for F_emP2 yields the interval estimate

$$[F_\mathrm{emP2}] = \frac{\left[\tilde{x}_1^{\langle \mathrm{A} \rangle}\right] - \left[\tilde{x}_1^{\langle \mathrm{B} \rangle}\right]}{2 \ln\left(\dfrac{\tilde{x}_3^{\langle \mathrm{A} \rangle}}{\tilde{x}_3^{\langle \mathrm{B} \rangle}}\right)} \ . \tag{7}$$

A backward substitution of this estimate into (6) then produces the second parameter estimate

$$[F_{\mathrm{emP1}}] = \frac{2mg}{\left(\tilde{x}_3^{\langle \mathrm{A} \rangle}\right)^2 \cdot e^{-\frac{\left[\tilde{x}_1^{\langle \mathrm{A} \rangle}\right]}{[F_{\mathrm{emP2}}]}}} \,. \tag{8}$$

A summary of these interval estimates, determined for five different positions of the sphere is given in Tabs. 1–3. Finally, a convex interval hull over all obtained results is formed for both parameters to obtain a robust interval parameterization of the system model. Fig. 2 gives a comparison of the resulting interval bounds for the force characteristic with a fixed current for either neglecting the uncertainty in the position measurement or for the interval-valued uncertainty model described above.

Table 1. Controlled operating points for five different test settings.

	Test n°1	Test n°2	Test n°3	Test n°4	Test n°5
$\mathrm{mid}\left(\left[\tilde{x}_1^{\langle \iota \rangle}\right]\right)$ in m	0.008	0.009	0.010	0.011	0.012
$\tilde{x}_3^{\langle \iota \rangle}$ in A	0.6045	0.6987	0.7476	0.8306	0.8820

Table 2. Estimates of F_{emP1} in $\mathrm{N \cdot m \cdot A^{-2}}$ at the interval midpoints $\mathrm{mid}\left(\left[\tilde{x}_1^{\langle \iota \rangle}\right]\right)$.

A \ B	Test n°1	Test n°2	Test n°3	Test n°4	Test n°5
Test n°1	/	0.1074	0.0789	0.0787	0.0735
Test n°2	–	/	0.0573	0.0629	0.0597
Test n°3	–	–	/	0.0781	0.0633
Test n°4	–	–	–	/	0.0506

Table 3. Estimates of F_{emP2} in m at the interval midpoints $\mathrm{mid}\left(\left[\tilde{x}_1^{\langle \iota \rangle}\right]\right)$.

A \ B	Test n°1	Test n°2	Test n°3	Test n°4	Test n°5
Test n°1	/	0.0034	0.0047	0.0047	0.0052
Test n°2	–	/	0.0074	0.0057	0.0064
Test n°3	–	–	/	0.0047	0.0060
Test n°4	–	–	–	/	0.0083

Identification of the Parameters of the Electrical Subsystem: The parameter identification in the second stage is performed by numerically minimizing the integral quadratic error between measured and simulated currents, where we assume that random measurement errors of the position and the electric current average out over sufficiently long measurement horizons (150 s) with a sampling period of 3 ms. After performining the minimization of the cost function with the help of a Nelder-Mead simplex method, a convex interval hull is again determined over several experiments with either constant positions x_1 or sinusoidal trajectories (including a transition from the initial equilibrium with vanishing voltage). This hull operation, cf. Tabs. 4 and 5, accounts for the systematic mismatch between the actual time constant and its approximation in terms of an interval representation. A visualization of the interval-based time constant model is given in Fig. 3.

Table 4. Interval bounds for the parameters of the mechanical subsystem model.

m in kg	F_{emP1} in $\mathrm{N \cdot m \cdot A^{-2}}$	F_{emP2} in m
0.0571	[0.0294 ; 0.2898]	[0.0026 ; 0.0104]

Table 5. Interval bounds for the parameters of the electrical subsystem model.

f_{ip1} in $\mathrm{m \cdot s}$	f_{ip2} in m
[0.0069 ; 0.0076]	[0.0071 ; 0.0293]
k_{i} in $\mathrm{A \cdot V^{-1}}$	c_{i} in A
[2.8713 ; 2.8974]	[−0.1532 ; −0.1464]

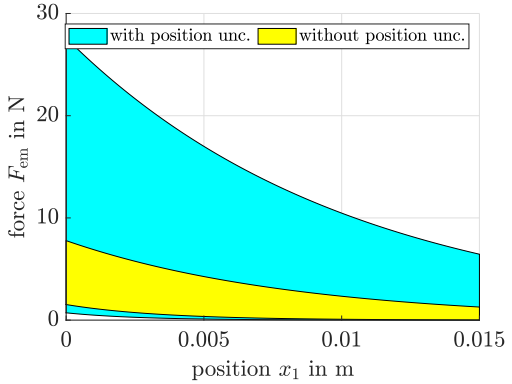

Fig. 2. Identification of the uncertainty of the position-dependent magnetic force characteristic $F_{\mathrm{em}}(x_1)$ for the electric current $x_3 = 0.5\,\mathrm{A}$.

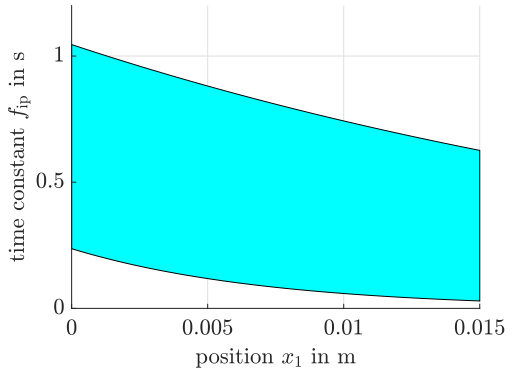

Fig. 3. Identification of the uncertainty of the position-dependent time constant $f_{\mathrm{ip}}(x_1)$.

3. STOCHASTIC AND ELLIPSOIDAL STATE ESTIMATION

For the state estimation procedures in this section, the system model of the magnetic levitation system is discretized by means of an explicit Euler method with the step size 3 ms. Moreover, additive process uncertainties are included in the discretized state equations, which are given by zero-mean Gaussian noise with the covariance $\mathbf{C_w}$ in the stochastic case and a suitable ellipsoid of a given confidence percentage in the set-valued counterpart. The measured system states $\mathbf{y}_{\mathrm{m},k+1}$ are the position and the electric current with the measurement covariance $\mathbf{C_v}$.

3.1 Unscented Kalman Filter

For the stochastic state estimation, a UKF according to Julier et al. (2000) is used which consists of an alternating evaluation of prediction and innovation steps.

To handle the nonlinearity in the state equations, $2n_\mathrm{x}$ sigma points are determined. These points are obtained by systematically adding increment vectors $\tilde{\mathbf{x}}^{(i)}$ onto the most recent expected value vector $\boldsymbol{\mu}^\mathrm{e}_{\mathbf{x},k}$ from the predecing innovation step according

$$\mathbf{x}^{(i)} = \boldsymbol{\mu}^\mathrm{e}_{\mathbf{x},k} + \tilde{\mathbf{x}}^{(i)} \ , \quad i \in \{1, \ldots, 2n_\mathrm{x}\} \ , \tag{9}$$

where

$$\tilde{\mathbf{x}}^{(i)} = \left(\sqrt{n_\mathrm{x}\mathbf{C}^\mathrm{e}_{\mathbf{x},k}}\right)^T_i \quad \text{and} \quad \tilde{\mathbf{x}}^{(n_\mathrm{x}+i)} = -\left(\sqrt{n_\mathrm{x}\mathbf{C}^\mathrm{e}_{\mathbf{x},k}}\right)^T_i \tag{10}$$

for $i \in \{1, \ldots, n_\mathrm{x}\}$; $\left(\sqrt{n_\mathrm{x}\mathbf{C}^\mathrm{e}_{\mathbf{x},k}}\right)_i$ denotes the i-th row of the matrix square root of the scaled symmetric positive-definite state covariance matrix of the innovation stage.

During the prediction step, the sigma points are individually propagated through the discretized model of the magnetic levitation system, yielding $\mathbf{x}^{\mathrm{p},(i)}_{k+1}$. With the help of these predicted sigma points $\mathbf{x}^{\mathrm{p},(i)}_{k+1}$, the new mean and covariance are obtained according to

$$\boldsymbol{\mu}^\mathrm{p}_{\mathbf{x},k+1} = \frac{1}{2n_\mathrm{x}} \sum_{i=1}^{2n_\mathrm{x}} \mathbf{x}^{\mathrm{p},(i)}_{k+1} \quad \text{and} \tag{11}$$

$$\mathbf{C}^\mathrm{p}_{\mathbf{x},k+1} = \frac{1}{2n_\mathrm{x}} \sum_{i=1}^{2n_\mathrm{x}} \left(\mathbf{x}^{\mathrm{p},(i)}_{k+1} - \boldsymbol{\mu}^\mathrm{p}_{\mathbf{x},k}\right)\left(\mathbf{x}^{\mathrm{p},(i)}_{k+1} - \boldsymbol{\mu}^\mathrm{p}_{\mathbf{x},k}\right)^T + \mathbf{C}_{\mathbf{w},k} \, . \tag{12}$$

Subsequently, the next innovation step is evaluated according to

$$\boldsymbol{\mu}^\mathrm{e}_{\mathbf{x},k+1} = \boldsymbol{\mu}^\mathrm{p}_{\mathbf{x},k+1} + \mathbf{L}_{k+1} \cdot \left(\mathbf{y}_{\mathrm{m},k+1} - \mathbf{C} \cdot \boldsymbol{\mu}^\mathrm{p}_{\mathbf{x},k+1}\right) \ , \tag{13}$$

$$\mathbf{C}^\mathrm{e}_{\mathbf{x},k+1} = (\mathbf{I} - \mathbf{L}_{k+1}\mathbf{C}) \cdot \mathbf{C}^\mathrm{p}_{\mathbf{x},k+1} \ , \tag{14}$$

where — due to the linearity of the measurement model $\mathbf{y}_{k+1} = \mathbf{C} \cdot \mathbf{x}_{k+1}$ — the time-varying gain matrix $\mathbf{L}_{k+1}$ is obtained as in the classical linear Kalman filter.

3.2 Ellipsoidal State Estimator

For the ellipsoidal state estimation, we assume that the set of reachable states is bounded at the time instant k by the ellipsoid

$$\begin{aligned} &\mathcal{E}_k\left(\boldsymbol{\mu}_k, \boldsymbol{\Gamma}_k\right) \\ &:= \left\{ \mathbf{x}_k \in \mathbb{R}^{n_\mathrm{x}} \;\middle|\; \left(\mathbf{x}_k - \boldsymbol{\mu}_k\right)^T \boldsymbol{\Gamma}_k^{-T} \boldsymbol{\Gamma}_k^{-1} \left(\mathbf{x}_k - \boldsymbol{\mu}_k\right) \leq 1 \right\} \end{aligned} \tag{15}$$

with the positive definite shape matrix

$$\mathbf{Q}_k = \boldsymbol{\Gamma}_k \boldsymbol{\Gamma}_k^T \succ 0 \tag{16}$$

(given in factorized form with the i-th column $\boldsymbol{\Gamma}_{i,k}$) and the midpoint vector $\boldsymbol{\mu}_k \in \mathbb{R}^{n_\mathrm{x}}$. As a generalization of the procedure derived by Rauh and Jaulin (2021), a simple ellipsoid state prediction procedure is given by the Algorithms 1 and 2, where we assume that the discrete-time system model is given by the expression $\mathbf{x}_{k+1} = \mathbf{f}\left(\mathbf{x}_k, u_k, \mathbf{p}\right)$ with the bounded parameters $\mathbf{p} \in [\mathbf{p}]$ according to the previous section.

For the applicability of the approach, the Jacobian

$$\mathbf{A}_k = \frac{\partial \mathbf{f}}{\partial \mathbf{x}_k}\left(\boldsymbol{\mu}_k, u_k, \check{\mathbf{p}}\right) \tag{17}$$

evaluated at the ellipsoid midpoint $\boldsymbol{\mu}_k$ and at the midpoint $\check{\mathbf{p}}$ of the interval box of the uncertain parameters is assumed to be invertible. The interval extension of the Jacobian required in Algorithm 2 is denoted by $[\mathbf{J}_\mathbf{f}]$.

Algorithm 1: Ellipsoid state prediction step

input : $\mathbf{f}\left(\mathbf{x}_k, u_k, \mathbf{p}\right)$, $\{\boldsymbol{\mu}_k, \boldsymbol{\Gamma}_k\}$, $[\mathbf{p}]$
output: $\{\boldsymbol{\mu}_{k+1}, \boldsymbol{\Gamma}_{k+1}\}$

$\boldsymbol{\mu}_{k+1} = \mathbf{f}\left(\boldsymbol{\mu}_k, u_k, \check{\mathbf{p}}\right)$
$\mathbf{A}_k = \frac{\partial \mathbf{f}}{\partial \mathbf{x}_k}\left(\boldsymbol{\mu}_k, u_k, \check{\mathbf{p}}\right)$
$\boldsymbol{\Gamma}_{k+1} = \mathbf{A}_k \cdot \boldsymbol{\Gamma}_k$
$\rho_k \leftarrow$ **Compute norm** of the linearization error
$\boldsymbol{\Gamma}_{k+1} := (1 + \rho_k) \cdot \boldsymbol{\Gamma}_{k+1}$

Algorithm 2: Compute norm of the linearization error

input : $\boldsymbol{\mu}_k, \boldsymbol{\Gamma}_k, \boldsymbol{\Gamma}_{k+1}$
output: ρ_k

$[x_{i,k}] = \mu_{i,k} + \left\|\boldsymbol{\Gamma}^T_{i,k}\right\| \cdot [-1 \ ; \ 1] \ , \quad i \in \{1, \ldots, n_\mathrm{x}\}$
$[\mathbf{x}_k] = [x_{1,k}] \times \ldots \times [x_{n,k}]$
$[\mathbf{J}_\mathbf{f}] = \left[\frac{\partial \mathbf{f}}{\partial \mathbf{x}_k}\right]\left([\mathbf{x}_k], u_k, [\mathbf{p}]\right)$
$\left[\tilde{\mathbf{b}}_k\right] = \left(\boldsymbol{\Gamma}^{-1}_{k+1} \cdot [\mathbf{J}_\mathbf{f}] \cdot \boldsymbol{\Gamma}_k - \mathbf{I}\right) \cdot [-1 \ ; \ 1]_{\times n}$
$\rho_k = \sup\left\{\left\|\left[\tilde{\mathbf{b}}_k\right]\right\|\right\}$

The predicted ellipsoid with the shape matrix $\boldsymbol{\Gamma}_{k+1} \cdot \boldsymbol{\Gamma}^T_{k+1}$ is then inflated by means of

$$\mathbf{Q}_{k+1} := \left(1 + \frac{1}{\beta}\right) \cdot \left(\boldsymbol{\Gamma}_{k+1} \cdot \boldsymbol{\Gamma}^T_{k+1}\right) + (1 + \beta) \cdot \mathbf{Q}_\mathbf{w} \tag{18}$$

with the factor

$$\beta = \sqrt{\frac{\operatorname{trace}\left\{\boldsymbol{\Gamma}_{k+1} \cdot \boldsymbol{\Gamma}^T_{k+1}\right\}}{\operatorname{trace}\left\{\mathbf{Q}_\mathbf{w}\right\}}} \tag{19}$$

determined according to Kurzhanskii and Vályi (1997); Noack et al. (2009), where $\mathbf{Q}_\mathbf{w} = r^2_\mathbf{w} \cdot \mathbf{C}_\mathbf{w}$ is the confidence ellipsoid related to the process noise with the inflation factor $r_\mathbf{w}$ chosen as described in Wang et al. (2015).

In the set-based innovation step, an intersection of the predicted ellipsoid with the measurements described by the set-based model

$$\left(\mathbf{x}_{k+1} - \mathbf{y}'_{\mathrm{m},k+1}\right)^T \cdot \mathbf{P}'_\mathrm{m} \cdot \left(\mathbf{x}_{k+1} - \mathbf{y}'_{\mathrm{m},k+1}\right) \leq 1 \tag{20}$$

is performed.

In the inequality (20), the matrix $\mathbf{P}'_\mathrm{m}$ is a purely diagonal matrix if the system's output matrix $\mathbf{C}$ in the measurement equation

$$\mathbf{y}_{k+1} = \mathbf{C} \cdot \mathbf{x}_{k+1} \tag{21}$$

represents a direct measurement of selected components of the state vector $\mathbf{x}_{k+1}$, i.e., being an all-zero matrix except for a single entry with the value one per row. If less outputs than state variables are available as measured data, Eq. (20) is a degenerate ellipsoid in which the matrix $\mathbf{P}'_\mathrm{m}$ is not invertible.

Using this notation, $\mathbf{y}'_{\mathrm{m},k+1}$ is an augmented measurement vector in which entries that correspond to non-measured components of the state vector at the time instant $k+1$ are set to the associated predicted ellipsoid midpoint $\boldsymbol{\mu}_{k+1}$. For a detailed description of the intersection procedure of two ellipsoids with different midpoints, the reader is referred to Sec. 3.2.2 in Rauh et al. (2021).

4. ESTIMATION RESULTS

To validate both the stochastic and set-valued state estimators, identical experimental data are used in all following evaluations. The data were generated for the test rig in Fig. 1 with the control voltage depicted in Fig. 4. This signal stems from a heuristically tuned PID controller with a sinusoidal desired variation of the sphere position.

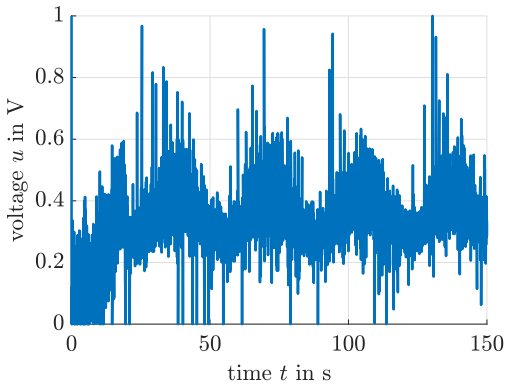

Fig. 4. Control signal $u(t)$ for the experimental validation.

For a direct application of the UKF, all interval parameters discussed before are replaced by their midpoints. Then, the diagonal covariance matrices (given in terms of SI units)

$$\begin{aligned}\mathbf{C_w} &= \operatorname{diag}\left\{\left[3\cdot10^{-9}\ \ 7.5\cdot10^{-4}\ \ 3\cdot10^{-5}\right]\right\} \quad \text{and}\\ \mathbf{C_v} &= \operatorname{diag}\left\{\left[1.44\cdot10^{-8}\ \ 2.5\cdot10^{-3}\right]\right\}\ ,\end{aligned} \tag{22}$$

where $\mathbf{C_w}$ has been tuned heuristically and $\mathbf{C_v}$ chosen according to the actual measurement uncertainty, yield the estimation results in Fig. 5. Although this estimator is capable of filtering the noisy position and current measurements, it obviously fails to estimate the sphere velocity consistently (its actual mean must be close to zero to reflect the sphere motion with constant amplitude) as the true velocity is mostly not even included in the depicted 3-standard deviation bounds in Fig. 5(b). This shortcoming can be removed if the system model is extended according to

$$\begin{aligned}\dot{x}_1 &= x_2\\ \dot{x}_2 &= -\frac{F_{\mathrm{em}}(x_1,x_3)+x_4}{2m}+g\\ \dot{x}_3 &= \frac{1}{f_{\mathrm{ip}}(x_1)}(k_{\mathrm{i}}\cdot u+c_{\mathrm{i}}-x_3)\\ \dot{x}_4 &= 0\ ,\end{aligned} \tag{23}$$

by including an integrator disturbance model for the disturbance force x_4, representing the mismatch between the model and the real dynamics (cf. Fig. 6).

Finally, the use of the ellipsoidal approach in Fig. 7 yields estimates for the velocity in Fig. 7(b) which enclose the physically meaningful solution without the need to include additional disturbance state variables. All covariance matrices used before have been replaced by ellipsoids in this case that correspond to a 95% confidence level of the corresponding Gaussian probability density.

5. CONCLUSIONS AND FUTURE WORK

In this paper, an ellipsoidal state estimation algorithm has been presented and validated experimentally against a UKF for state estimation of a magnetic levitation system. It has been shown that the proposed interval representation of state-dependent nonlinearities allows for obtaining a robust model that leads to a state estimation scheme that has comparable complexity as a UKF but much higher consistency of the results. Future work will aim at extensions toward the online identification of uncertain parameters by the proposed ellipsoidal framework as well as its use in model-predictive control procedures.

REFERENCES

Balko, P. and Rosinova, D. (2017). Modeling of Magnetic Levitation System. In *Proc. of 21st International Conference on Process Control (PC)*, 252–257. Strbske Pleso, Slovakia.

Efimov, D., Raïssi, T., Chebotarev, S., and Zolghadri, A. (2013). Interval State Observer for Nonlinear Time Varying Systems. *Automatica*, 49(1), 200–205.

INTECO Sp. z o. o. (n.a.). Magnetic Levitation System. `http://www.inteco.com.pl/products/magnetic-levitation-systems/`, accessed: Nov. 08, 2022.

Julier, S., Uhlmann, J., and Durrant-Whyte, H. (2000). A New Approach for the Nonlinear Transformation of Means and Covariances in Filters and Estimators. *IEEE Transactions on Automatic Control*, 45(3), 477–482.

Kletting, M., Rauh, A., Aschemann, H., and Hofer, E. (2006). Interval Observer Design for Nonlinear Systems with Uncertain Time-Varying Parameters. In *Proceedings of 12th IEEE International Conference on Methods and Models in Automation and Robotics MMAR*, 361–366. Miedzyzdroje, Poland.

Krämer, W. (n.a.). XSC Languages (C-XSC, PASCAL-XSC) — Scientific Computing with Validation, Arithmetic Requirements, Hardware Solution and Language Support. `http://www.math.uni-wuppertal.de/ xsc/`, accessed: Nov. 08, 2022.

Kurzhanskii, A.B. and Vályi, I. (1997). *Ellipsoidal Calculus for Estimation and Control*. Birkhäuser, Boston, MA.

Lohner, R.J. (2001). *On the Ubiquity of the Wrapping Effect in the Computation of Error Bounds*, 201–216. Springer–Verlag, Vienna.

Noack, B., Klumpp, V., and Hanebeck, U. (2009). State Estimation with Sets of Densities Considering Stochastic and Systematic Errors. In *2009 12th International Conference on Information Fusion, FUSION 2009*, 1751–1758. Seattle, WA, USA.

Puig, V., Stancu, A., and Quevedo, J. (2005). Observers for Interval Systems using Set and Trajectory-based Approaches. In *Proc. of the 44th IEEE Conference on Decision and Control and European Control Conference, CDC-ECC'05*, 6567–6572. Seville, Spain.

Rauh, A., Bourgois, A., and Jaulin, L. (2021). Union and Intersection Operators for Thick Ellipsoid State Enclosures: Application to Bounded-Error Discrete-Time State Observer Design. *Algorithms*, 14(3), 88.

Rauh, A. and Jaulin, L. (2021). A Computationally Inexpensive Algorithm for Determining Outer and Inner

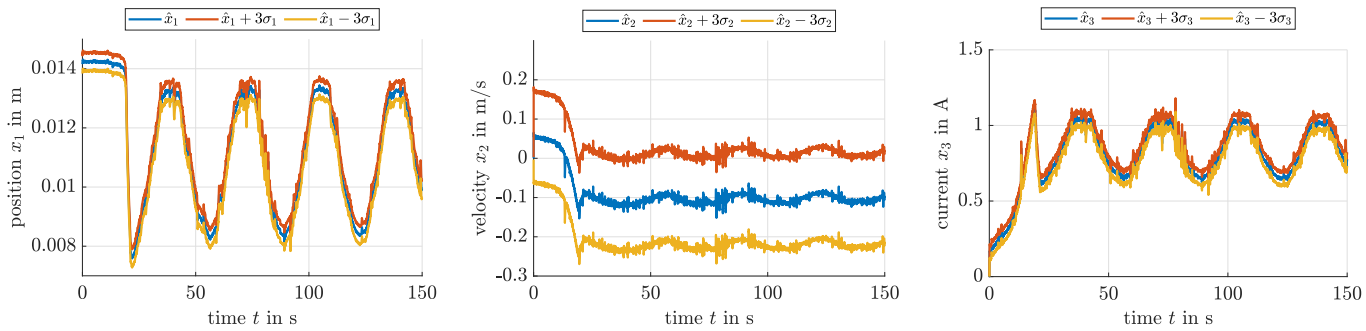

(a) Estimated position x_1. (b) Estimated velocity x_2. (c) Estimated current x_3.

Fig. 5. State estimate for a UKF without disturbance estimation; interval parameters are replaced with their midpoints.

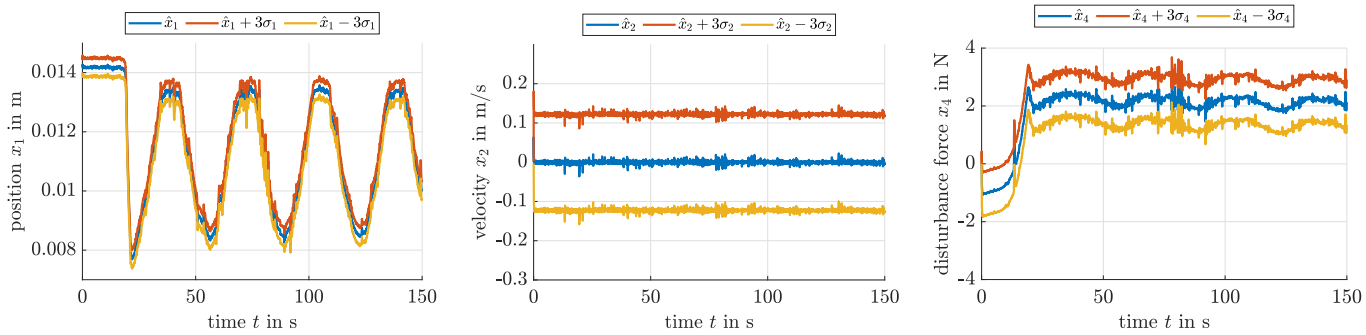

(a) Estimated position x_1. (b) Estimated velocity x_2. (c) Estimated disturbance x_4.

Fig. 6. State estimate for a UKF with disturbance estimation using the model (23); interval parameters are replaced with their midpoints.

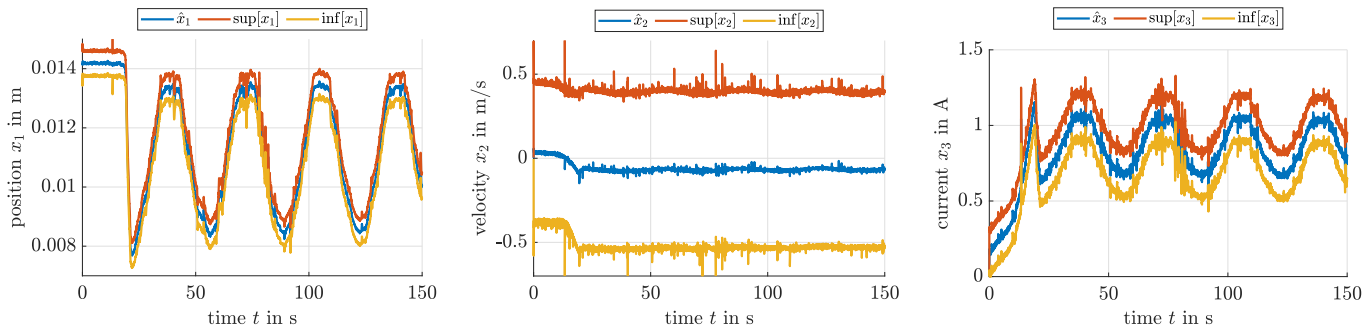

(a) Estimated position x_1. (b) Estimated velocity x_2. (c) Estimated current x_3.

Fig. 7. Bounds for the ellipsoidal estimator with interval-based models for $F_{\mathrm{em}}(x_1)$ and $f_{\mathrm{ip}}(x_1)$.

Enclosures of Nonlinear Mappings of Ellipsoidal Domains. *International Journal of Applied Mathematics and Computer Science AMCS*, 31(3), 399–415.

Rauh, A. and Kersten, J. (2021). Transformation of Uncertain Linear Systems with Real Eigenvalues into Cooperative Form: The Case of Constant and Time-Varying Bounded Parameters. *Algorithms*, 14(3).

Rego, B., Locatelli, D., Raimondo, D., and Raffo, G. (2022). Joint State and Parameter Estimation Based on Constrained Zonotopes. *Automatica*, 142, 110425.

Rohou, S. and Jaulin, L. (2021). Exact Bounded-Error Continuous-Time Linear State Estimator. *Systems & Control Letters*, 153, 104951.

Rosinova, D. and Hypiusova, M. (2021). Comparison of Nonlinear and Linear Controllers for Magnetic Levitation System. *Applied Sciences*, 11, 7795.

Rump, S. (1999). INTLAB — INTerval LABoratory. In T. Csendes (ed.), *Developments in Reliable Computing*, 77–104. Kluver Academic Publishers.

Smith, H. (1995). *Monotone Dynamical Systems: An Introduction to the Theory of Competitive and Cooperative Systems*, volume 41. Mathematical Surveys and Monographs, American Mathematical Soc., Providence.

Wang, B., Shi, W., and Miao, Z. (2015). Confidence Analysis of Standard Deviational Ellipse and Its Extension into Higher Dimensional Euclidean Space. *PLOS ONE*, 10(3), 1–17.

Wang, Z., Lim, C.C., and Shen, Y. (2018). Interval Observer Design for Uncertain Discrete-Time Linear Systems. *Systems & Control Letters*, 116, 41–46.